

Light-Driven Spatiotemporal Pickering Emulsion Droplet Manipulation Enabled by Plasmonic Hybrid Microgels

Xin Guan, Guangyao Cheng, Yi-Ping Ho,* Bernard P. Binks,* and To Ngai*

The past decades have witnessed the development of various stimuli-responsive materials with tailored functionalities, enabling droplet manipulation through external force fields. Among different strategies, light exhibits excellent flexibility for contactless control of droplets, particularly in three-dimensional space. Here, we present a facile synthesis of plasmonic hybrid microgels based on the electrostatic heterocoagulation between cationic microgels and anionic Au nanoparticles. The hybrid microgels are effective stabilizers of oil-in-water Pickering emulsions. In addition, the laser irradiation on Au nanoparticles creates a “cascade effect” to thermally responsive microgels, which triggers a change in microgel wettability, resulting in microgel desorption and emulsion destabilization. More importantly, the localized heating generated by a focused laser induces the generation of a vapor bubble inside oil droplets, leading to the formation of a novel air-in-oil-in-water (A/O/W) emulsion. These A/O/W droplets are able to mimic natural microswimmers in an aqueous environment by tracking the motion of a laser spot, thus achieving on-demand droplet merging and chemical communication between isolated droplets. Such proposed systems are expected to extend the applications of microgel-stabilized Pickering emulsions for substance transport, programmed release and controlled catalytic reactions.

1. Introduction

Particle-stabilized emulsions, known as Pickering emulsions, are highly stable systems because particles are more or less irreversibly adsorbed onto the oil-water interfaces due to their high desorption energy.^[1,2] Compared with rigid particles, microgels have emerged as a promising emulsifier for stabilizing emulsions because they are soft and deformable and can spontaneously adsorb at the oil-water interface to reduce the interfacial tension and form a steric barrier.^[3–5] Typically, microgels are hydrophilic and tend to swell in an aqueous solution.^[6] Among different types of microgels, poly(N-isopropylacrylamide) or PNIPAM-based microgels are typically used as thermo-responsive materials with a low critical solution temperature (LCST) at ≈ 32 °C.^[7] Owing to the reconfigurable hydrogen bonding between the polymer molecules and water molecules, PNIPAM blocks undergo significant size reduction and transition from hydrophilic to hydrophobic at temperatures

X. Guan, T. Ngai
Department of Chemistry
The Chinese University of Hong Kong
Shatin, N.T., Hong Kong China
E-mail: tongai@cuhk.edu.hk

G. Cheng, Y.-P. Ho
Department of Biomedical Engineering
The Chinese University of Hong Kong
Shatin, N.T., Hong Kong China
E-mail: ypho@cuhk.edu.hk

Y.-P. Ho
Centre for Novel Biomaterials
The Chinese University of Hong Kong
Shatin, N.T., Hong Kong China

Y.-P. Ho
Hong Kong Branch of CAS Center for Excellence
in Animal Evolution and Genetics
The Chinese University of Hong Kong
Shatin, N.T., Hong Kong China

Y.-P. Ho
The Ministry of Education Key Laboratory of Regeneration Medicine
The Chinese University of Hong Kong
Shatin, N.T., Hong Kong China

Y.-P. Ho
State Key Laboratory of Marine Pollution
City University of Hong Kong
Kowloon, Hong Kong China

B. P. Binks
Department of Chemistry
University of Hull
Hull HU6 7RX, UK
E-mail: b.p.binks@hull.ac.uk



The ORCID identification number(s) for the author(s) of this article can be found under <https://doi.org/10.1002/smll.202304207>

© 2023 The Authors. Small published by Wiley-VCH GmbH. This is an open access article under the terms of the Creative Commons Attribution License, which permits use, distribution and reproduction in any medium, provided the original work is properly cited.

DOI: 10.1002/smll.202304207

above the LCST.^[8–10] Therefore, PNIPAM-based microgel-stabilized emulsions are thermally sensitive and can be demulsified by increasing the temperature.^[11]

Although it is possible to alter the structure and properties of microgels by changing the type of comonomers or the conditions of polymerization,^[12] conventional microgels are limited for particular applications due to the absence of specific functionality or active sites. To this end, hybrid microgels have been proposed as a new generation of smart materials for applications in many fields, such as catalysis, biosensing, delivery systems and cell culture.^[13–17] By incorporating microgels with other kinds of material, the hybrid microgels may combine properties from an array of components providing complex structures and multi-functionality.^[18–22] In particular, the hybridization between metal nanoparticles and microgels has received much attention in recent years.^[23–26] First, metal nanoparticles impart microgels and microgel-stabilized emulsions with desirable functionalities, such as magnetic responsiveness and catalytic activity.^[27–29] Additionally, embedding metal nanoparticles into microgel networks may create a “cascade effect,” where an external stimulus induced response of the metal nanoparticles may be cascaded to the microgels.^[30] For example, plasmonic hybrid microgels containing Au nanoparticles (either Au nanoparticle core-microgel shell or microgel core-Au nanoparticle shell) are capable of converting light energy into thermal energy, resulting in hydration to dehydration transition of the microgels and alteration of surface friction.^[31,32]

Owing to the advantages of large interfacial area and small size, emulsion droplets have been developed as micro-reactors for multiple biochemical reactions.^[33–36] However, most of the current systems have focused on improving the catalytic efficiency at the oil-water interface, lacking control of the whole reaction process and the chemical communication between droplets. To manipulate droplets, for example, through merging, external force fields such as electric and magnetic fields are typically required.^[37,38] Among the currently presented strategies, optical manipulation has drawn greater attention as the laser beam can be precisely focused on a specific place in an on-demand manner, allowing a spatiotemporal control of microdroplets.^[39–41] For example, an optical tweezer is capable of precisely and intuitively trapping and moving droplets in three-dimensional (3D) space, although only small droplets (<10 μm) can be efficiently trapped by a high power laser.^[42] Light-induced capillary effect and photothermal effect are alternative strategies for droplet manipulation.^[43,44] However, most of the produced droplets are stabilized by surfactant molecules, exhibiting low photothermal efficiency and requiring long irradiation time. Although plasmonic nanoparticles may function as light-to-heat converters under specific wavelengths, the fast and efficient light-mediated response of plasmonic nanoparticle-stabilized Pickering emulsions remains largely unexplored.^[45,46] In addition, it is still challenging to initiate reactions or the interaction of Pickering emulsion droplets containing different reagents by droplet merging or directed inter-droplet transportation.

In this work, a facile strategy is proposed to synthesize plasmonic hybrid microgels (Au@PNIPAM-*co*-ALA) consisting of a cationic poly(N-isopropylacrylamide-*co*-allylamine), PNIPAM-*co*-ALA, microgel core and a shell of multiple anionic Au nanoparticles by electrostatic heterocoagulation. Such hybrid microgels

combine the properties of microgels and Au nanoparticles, allowing the preparation of a novel class of photo-responsive oil-in-water (O/W) Pickering emulsions. Due to their strong plasmonic photothermal effect, the Au nanoparticles can convert light into thermal energy, leading to a significant increase in the surrounding temperature at the droplet interface. The thermally responsive microgels become collapsed, transiting from hydrophilic to hydrophobic with distinct interfacial behavior upon triggering by light. By altering the power, beam waist and irradiation time of the focused laser, instantaneous demulsification, droplet merging and bubble generation within droplets can be precisely controlled. The observed phenomena are then utilized to induce the content exchange between adjacent droplets and manipulate droplet movement, demonstrating the potential of applying the proposed system for the rational design of an artificial microswimmer or a smart microreactor that requires spatiotemporal control.

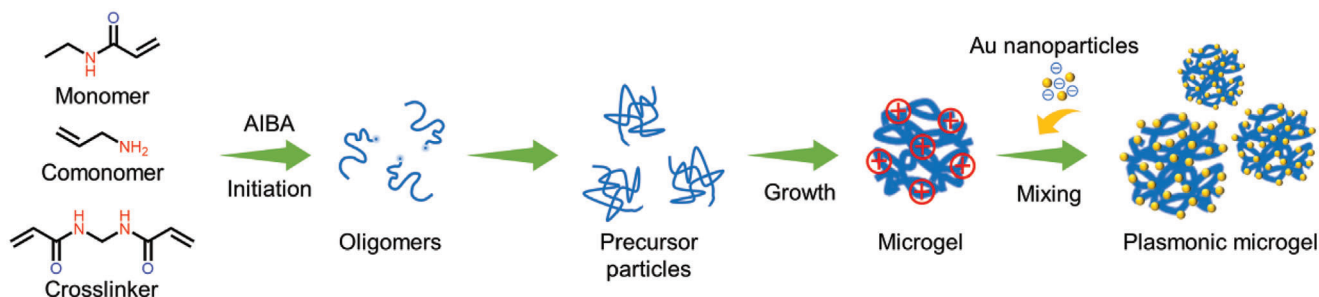
2. Results and Discussion

2.1. Design and Synthesis of Plasmonic Hybrid Microgels

As illustrated in **Scheme 1**, the formation of plasmonic hybrid microgels was designed as a three-step process based upon the heterocoagulation between oppositely charged PNIPAM-*co*-ALA microgels and citrate-stabilized Au nanoparticles. First, cationic PNIPAM-*co*-ALA microgels with an appropriate content of amino groups were synthesized through conventional free-radical precipitation polymerization in an aqueous solution. In parallel, anionic Au nanoparticles were synthesized by citrate reduction and stabilization. The hybrid Au@PNIPAM-*co*-ALA microgels were then easily produced *via* electrostatically driven co-assembly by mixing the two above-mentioned oppositely charged entities at suitable concentrations followed by removing excess Au nanoparticles by centrifugation.

2.2. Morphology and Chemical Composition of Hybrid Microgels

Scanning electron microscopy (SEM) and atomic force microscopy (AFM) were used to characterize the morphology and height profile of bare PNIPAM-*co*-ALA microgels and hybrid microgels (**Figure 1a–d**). As microgels are soft colloids and can be swollen by water molecules in an aqueous solution, dehydration and size variation were observed during the drying process. As seen in **Figure 1a–d**, neither kind of microgels appeared spherical on a silicon substrate. Specifically, bare PNIPAM-*co*-ALA microgels were observed to be smaller in diameter (600 nm) with a smoother surface compared to hybrid microgels (1 μm) with a rougher surface. As shown in the 3D AFM images and corresponding height profiles (**Figure 1e–g**), the maximum dry height of bare PNIPAM-*co*-ALA microgels was ≈110 nm, two times that of hybrid microgels (52 nm). We suspect that the dense packing of multiple Au nanoparticles on the microgel surface may lead to a higher density of cross-linked polymer networks in the microgel matrix due to the enhanced gravitational effect. As a result, additional pressure would be applied to microgels during the drying process, leading to a flat and lower height profile on



Scheme 1. Schematic illustration of the synthesis of plasmonic hybrid microgels with multiple Au nanoparticles on the surface.

the substrate. In addition, similar to the effect of plasma treatment on the substrate,^[47] the Au nanoparticle-coated microgels showed improved hydrophilicity, which increased the affinity between microgels and the substrate, resulting in a better stretch of polymer chains on the silicon wafer. On the other hand, the coating of Au nanoparticles may slow down the evaporation rate of absorbed water from the microgel matrix, thus forming a more homogeneous topography after drying.

The chemical composition of Au nanoparticles, PNIPAM-*co*-ALA microgels and hybrid microgels was analyzed by Fourier-transform infrared (FTIR) spectroscopy (Figure S1, Supporting Information). Specifically, the FTIR spectrum for Au nanoparticles shows sharp peaks ≈ 1410 and 1590 cm^{-1} related to symmetric and asymmetric stretching of COO^- groups in trisodium citrate, indicating that citrate ions were adsorbed on the surface of Au nanoparticles. The adsorption peaks at 1388 , 1368 , and 1172 cm^{-1} in the FTIR spectrum for PNIPAM-*co*-ALA microgels were related to the vibration of the $\text{CH}(\text{CH}_3)_2$ groups in the PNIPAM skeleton. In the range between 1600 and 1700 cm^{-1} , the stretching vibrations of the $\text{C}=\text{O}$ and $\text{C}-\text{N}$ groups were observed. The adsorption peak of in-plane N-H bending and N-H stretching vi-

bration can be found ≈ 1545 and 3250 cm^{-1} . Besides, the C-H bonds within microgels present an adsorption peak at $\approx 2900\text{ cm}^{-1}$. As the FTIR spectrum of hybrid microgels possesses the characteristic adsorption peaks from both PNIPAM-*co*-ALA microgels and Au nanoparticles, the successful formation of hybrid microgels consisting of Au nanoparticles and PNIPAM-*co*-ALA microgels was proved.

2.3. Thermally Reversible Swelling/Collapse of Microgels

To evaluate the thermal responsivity of microgels before and after hybridization, dynamic light scattering (DLS) was employed to measure their hydrodynamic size at different temperatures. As shown in **Figure 2a,b**, both PNIPAM-*co*-ALA and Au@PNIPAM-*co*-ALA microgels exhibit a decrease in size with increasing temperature from 20 to $40\text{ }^\circ\text{C}$, suggesting that the Au nanoparticles entrapped in the microgel matrix did not affect the thermal responsiveness of PNIPAM-*co*-ALA microgels. Furthermore, significant size reduction was observed near the LCST ($\approx 32\text{ }^\circ\text{C}$) for both microgels. Upon decreasing temperature, the microgels recovered to their swollen state with a concomitant increase in

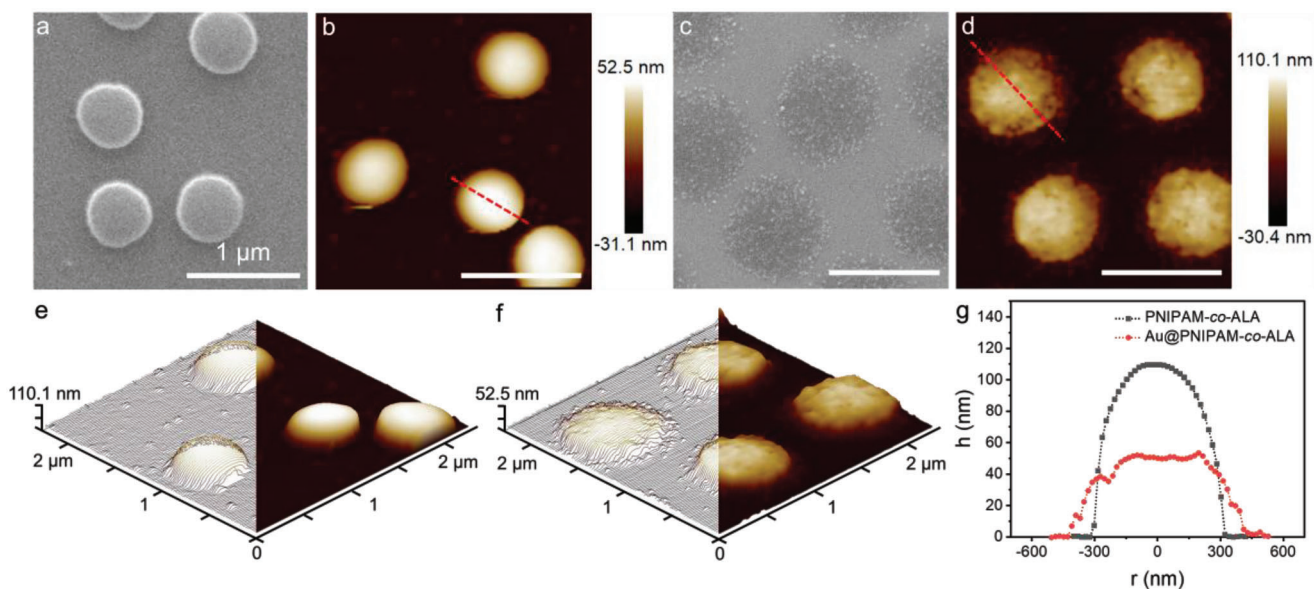


Figure 1. SEM and representative AFM height images of a,b) bare PNIPAM-*co*-ALA microgels and c,d) hybrid Au@PNIPAM-*co*-ALA microgels. 3D AFM images with wire plots of e) bare PNIPAM-*co*-ALA microgels and f) hybrid Au@PNIPAM-*co*-ALA microgels. g) Height profiles along the red line in (b) and (d) of a bare PNIPAM-*co*-ALA microgel and a hybrid Au@PNIPAM-*co*-ALA microgel, respectively on a silicon wafer.

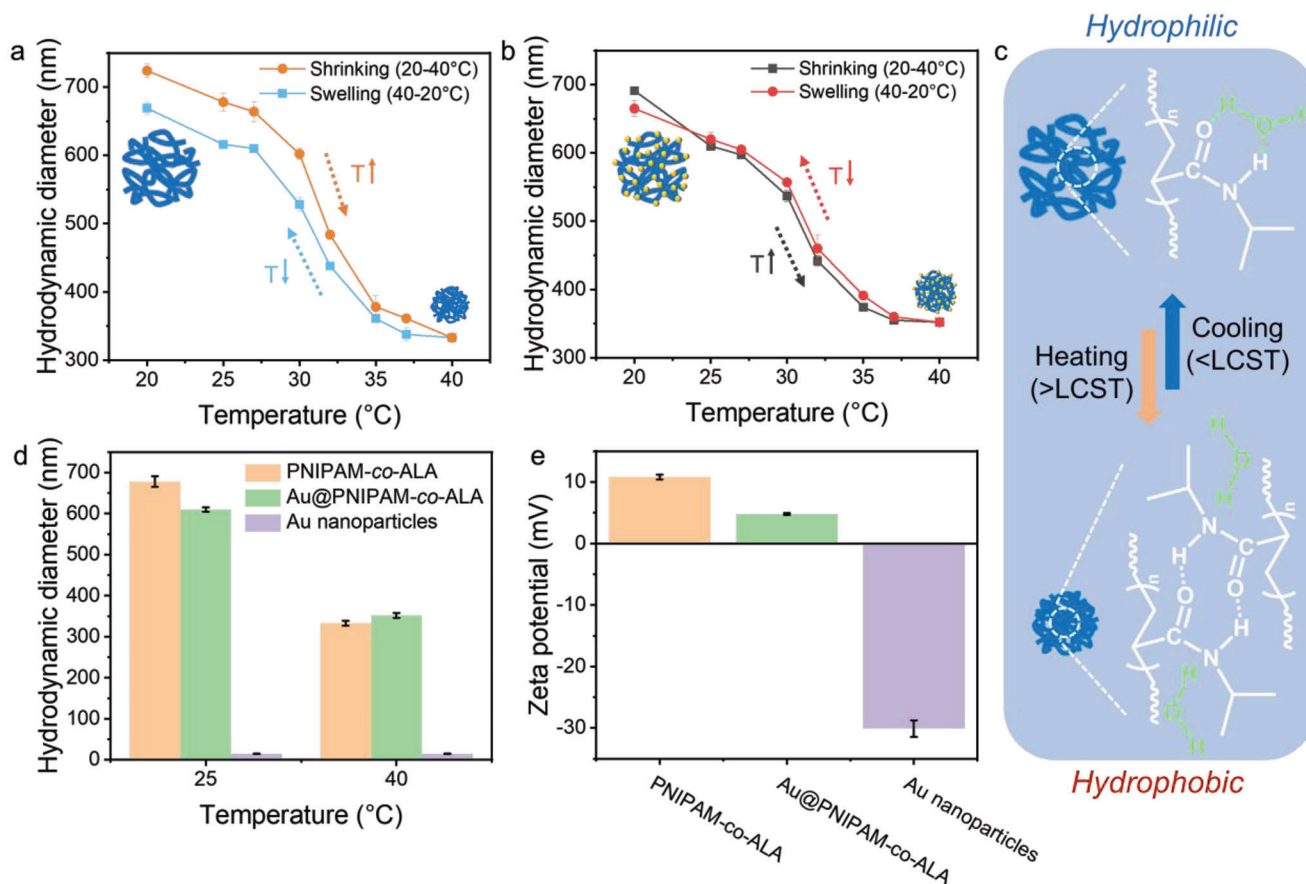


Figure 2. Temperature-induced changes in hydrodynamic diameter for a) PNIPAM-co-ALA microgels and b) Au@PNIPAM-co-ALA microgels dispersed in an aqueous solution. The heating (volume shrinking) and cooling (volume swelling) cycles are as indicated in the plots. c) Schematic illustration of microgel size reduction and hydrophilic to hydrophobic transition at temperatures above the LCST. d) Hydrodynamic diameter of Au nanoparticles, PNIPAM-co-ALA microgels and Au@PNIPAM-co-ALA microgels measured at 25 and 40 °C. e) Zeta potential of Au nanoparticles, PNIPAM-co-ALA microgels and Au@PNIPAM-co-ALA microgels in an aqueous solution at 25 °C.

size. The mechanism of the reversible swelling and shrinking of microgels is illustrated in Figure 2c. At temperatures below the LCST, water molecules can form a stable solvation cage around both hydrophilic and hydrophobic segments of microgels, keeping the microgels in a hydrated and swollen state. On the other hand, increasing the temperature above the LCST, the solvation cage is unstable and the hydrophobic intermolecular attractions become predominant, resulting in a significant collapse of the polymer network.

Interestingly, although Au@PNIPAM-co-ALA microgels were covered by multiple Au nanoparticles, their hydrodynamic size at room temperature appeared smaller compared to that of bare PNIPAM-co-ALA microgels as shown in Figure 2d. However, the size of hybrid microgels was larger than that of bare PNIPAM-co-ALA microgels at 40 °C. When the temperature increased from 25 to 40 °C, the temperature-triggered swelling ratios of bare and hybrid microgels were calculated to be 2.04 and 1.73, respectively. We suppose this is because the charge neutralization between oppositely charged Au nanoparticles and microgels may lead to a slight collapse of the outermost polymer matrix upon decreasing the electrostatic repulsion. At a temperature above the LCST, the influence of charge neutralization on particle size is presumably

insignificant. Although both bare and hybrid microgels shrink significantly, the larger size of hybrid microgels compared to bare microgels may be attributed to the adsorption of multiple Au nanoparticles on their surface. As evident in Figure 2e, the zeta potential of Au@PNIPAM-co-ALA microgels was measured to be 6–7 mV lower than that of bare PNIPAM-co-ALA microgels, in line with the anticipated partial charge neutralization between oppositely charged Au nanoparticles and PNIPAM-co-ALA microgels.

2.4. Structure and Properties of Hybrid Microgels

As the plasmonic photothermal effect mainly relies on the array of Au nanoparticles, the loading area and packing density of Au nanoparticles in the microgel matrix should be important influencing factors. To clarify the structure-function relationship of hybrid microgels, the hybrid microgel with a single Au nanoparticle core (S-Au@PNIPAM-co-ALA) was also synthesized based on the surface functionalization of citrate-stabilized anionic Au nanoparticles by cationic ALA molecules. The polymerization occurred from the surface of ALA-adsorbed Au nanoparticles and

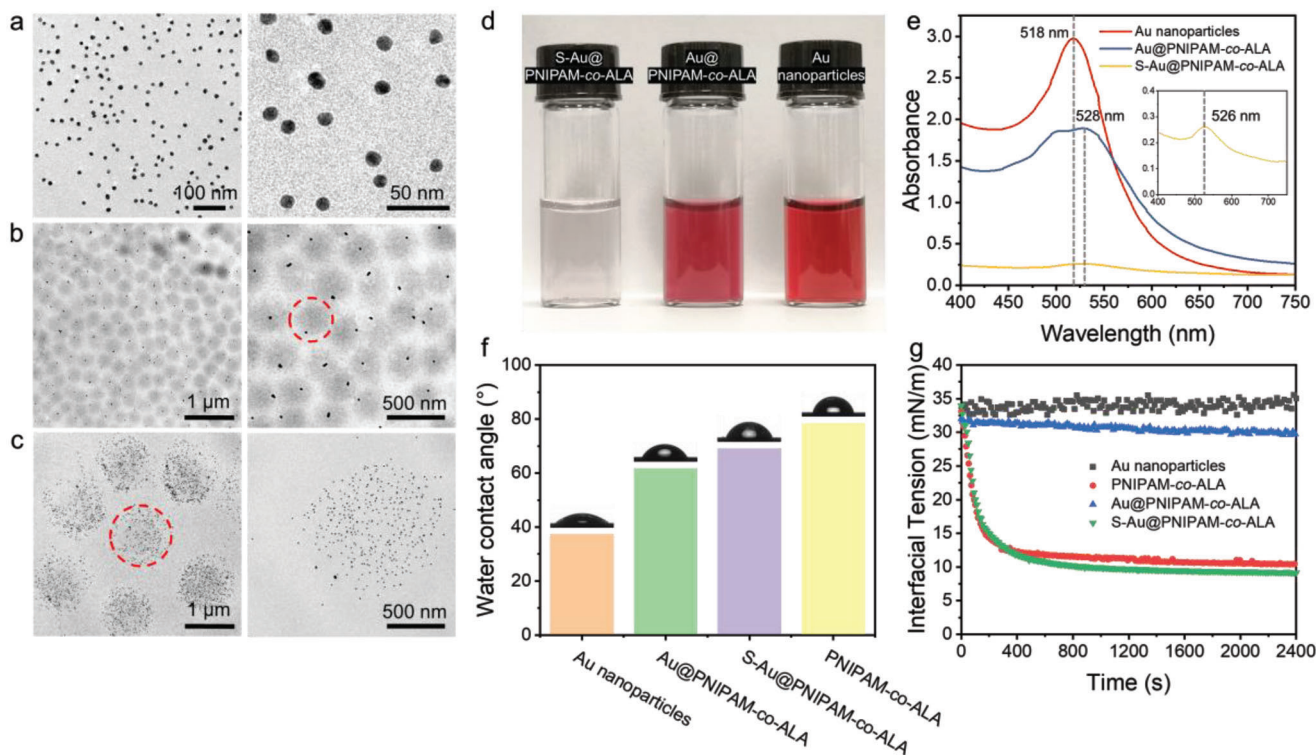


Figure 3. TEM images of a) Au nanoparticles, b) S-Au@PNIPAM-co-ALA microgels, and c) Au@PNIPAM-co-ALA microgels. d) Appearance of aqueous dispersions of Au nanoparticles, S-Au@PNIPAM-co-ALA microgels and Au@PNIPAM-co-ALA microgels. e) UV-vis absorption spectra of Au nanoparticles, S-Au@PNIPAM-co-ALA microgels and Au@PNIPAM-co-ALA microgels. f) Water contact angle of Au nanoparticles, PNIPAM-co-ALA microgels and hybrid microgels in air. g) Dynamic toluene-water interfacial tension in the presence of Au nanoparticles, PNIPAM-co-ALA microgels and hybrid microgels in water. Microgel concentration was 0.1 wt% in all samples.

gradually grew to form microgels with a single Au nanoparticle core.^[23] The diameter of Au nanoparticles was measured to be 12 nm and the dried single-core hybrid microgel was ≈ 350 nm in diameter (Figure 3a,b), smaller than bare PNIPAM-co-ALA microgels (Figure S2, Supporting Information). In contrast to the S-Au@PNIPAM-co-ALA microgel, more than 300 Au nanoparticles were adsorbed on the surface of a Au@PNIPAM-co-ALA microgel on average after heterocoagulation (Figure 3c).

Due to the different structures of synthesized hybrid microgels with either a single Au nanoparticle or multiple Au nanoparticles on their surfaces, we further explored their physical properties including light absorption, wettability and interfacial activity. At the same microgel concentration, the Au@PNIPAM-co-ALA microgel dispersion displayed a much deeper red color than the S-Au@PNIPAM-co-ALA microgel dispersion (Figure 3d). As shown in the UV-vis absorption spectra (Figure 3e), the isotropic Au nanoparticles possess only one characteristic absorption peak at 518 nm, while the absorption peak of hybrid microgels shifted to 528 nm. The red shift of ≈ 10 nm in hybrid microgels may be attributed to the plasmonic coupling effect of Au nanoparticles in the microgel matrix and the slight aggregation of Au nanoparticles during the synthesis and hybridization process. Besides, Au@PNIPAM-co-ALA microgels exhibited a much stronger light absorption than S-Au@PNIPAM-co-ALA microgels, consistent with their appearance.

We also found that the hydrophilicity of Au@PNIPAM-co-ALA microgels was increased relative to that of bare PNIPAM-co-ALA microgels due to the incorporation of hydrophilic Au nanoparticles on their surface (Figure 3f). On the other hand, although the size and packing density of bare PNIPAM-co-ALA microgels and S-Au@PNIPAM-co-ALA microgels on the substrate were not the same, the difference in water contact angle was small. The presence of Au nanoparticles not only changed the surface hydrophilicity of microgels, but also limited their interfacial activity. Interfacial tension measurements at the toluene-water interface indicate that Au nanoparticles did not reduce the interfacial tension whereas both bare microgels and S-Au@PNIPAM-co-ALA microgels were able to reduce the interfacial tension in a relatively short time, showing high interfacial activity. The equilibrium interfacial tension was ≈ 10 mN m⁻¹, much lower than that of the bare toluene-water interface (≈ 35 mN m⁻¹). In comparison, Au@PNIPAM-co-ALA microgels exhibited limited capability in reducing the interfacial tension. This suggests that the presence of multiple rigid Au nanoparticles on microgels compromises their interfacial activity due to enhanced hydrophilicity and impaired softness.

The thermal stability of hybrid microgels is an important property to be considered for their use in potential applications. We evaluated the thermal stability of both bare and hybrid microgels based on thermal gravimetric analysis (TGA). As shown in Figure S3, Supporting Information, it is surprisingly found

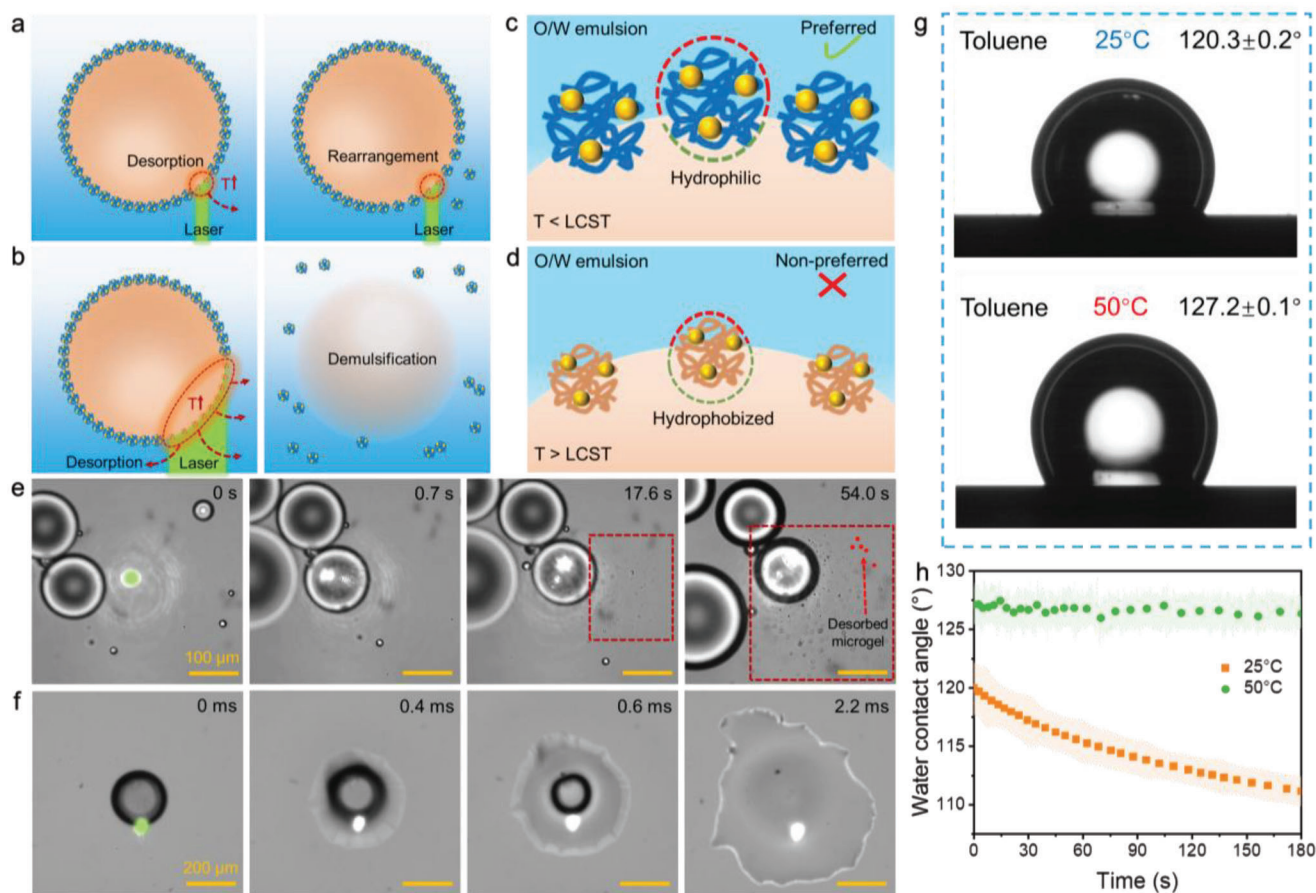


Figure 4. Schematic illustration of light-induced a) hybrid microgel desorption and b) demulsification of O/W Pickering emulsion. c,d) Proposed stabilization and destabilization mechanism of emulsion droplets depending on the wettability of microgels at different temperatures. e) Slow desorption of hybrid microgels from the oil-water interface induced by laser irradiation with a small beam waist (6 μm) and low power (8 mW). f) Rapid demulsification of an emulsion droplet irradiated by the laser with a larger beam waist (30 μm) and high power (20 mW). The green dot represents the localized laser beam. g) Appearance of a water drop on the substrate coated with Au@PNIPAM-co-ALA microgels in toluene at two temperatures. h) Change in contact angle as a function of time at two temperatures for Au@PNIPAM-co-ALA microgels.

that a small weight loss of 6%–8% occurred in the temperature range of 22–100 $^{\circ}\text{C}$. We suspect that was likely due to the evaporation of absorbed water in the microgel matrix. The decomposition temperature of the PNIPAM-co-ALA microgel was about 330 $^{\circ}\text{C}$. After heating to 500 $^{\circ}\text{C}$, weight loss of 80% was mainly attributed to the decomposition of the polymer skeleton and only 3% of the original weight remained. In comparison, the hybrid microgels showed improved thermal stability with a relatively higher decomposition temperature. A significant weight loss of Au@PNIPAM-co-ALA microgels occurred beyond 365 $^{\circ}\text{C}$ and the residual mass (<10%) of hybrid microgels was yielded in the studied temperature range (up to 500 $^{\circ}\text{C}$). Even though the decomposition of citrate ions on Au nanoparticle surfaces was inevitable, the larger residual mass of hybrid microgels than that of bare microgels after thermal degradation can be explained by the presence of adsorbed Au nanoparticles in hybrid microgels which cannot be decomposed at such a temperature (500 $^{\circ}\text{C}$). Hence, TGA results reveal that hybrid microgels showed enhanced thermal stability, allowing them to be used for potential applications at relatively high temperatures (<300 $^{\circ}\text{C}$).

2.5. Photothermal Response of Hybrid Microgels and Hybrid Microgel-Stabilized O/W Pickering Emulsions

Although Au@PNIPAM-co-ALA microgels could not reduce the interfacial tension as efficiently as bare PNIPAM-co-ALA microgels, they could still be used as an emulsion stabilizer. Compared to the bare PNIPAM-co-ALA microgel-stabilized O/W emulsion (Figure S4, Supporting Information), the O/W Pickering emulsion stabilized by Au@PNIPAM-co-ALA microgels possessed larger droplets as shown in Figure 4e. A customized optical setup (Figure S5, Supporting Information) was established to trigger the photothermal response of Au@PNIPAM-co-ALA microgels at oil droplet surfaces and simultaneously observe the behavior of microgel-stabilized O/W droplets upon irradiation by a focused 532 nm laser.

Before investigating the behavior of hybrid microgel-stabilized emulsion droplets under irradiation, we first evaluated the photothermal response of the hybrid microgel itself. As shown in Figure S6a, Supporting Information, the hybrid microgel dispersion was irradiated by a 532 nm laser with different power, during which a thermocouple immersed in the dispersion measured

the temperature variation and converted it into electrical data, allowing recording and analysis by a computer. We also investigated the effect of laser power and microgel concentration on the dispersion temperature. Figure S6b, Supporting Information shows that hybrid microgels can effectively convert light energy into heat, thus leading to a temperature increase with irradiation time. In comparison, the temperature of a bare microgel dispersion underwent almost no change during irradiation, which means bare microgels did not show any photothermal response. In addition, higher laser power and higher concentration of hybrid microgels resulted in a larger temperature increase due to enhanced light adsorption.^[48] It should be noted that the light-to-heat conversion was confined in a limited space surrounding hybrid microgels. The combined effect of low microgel concentrations (0.1–1 wt%), low laser energy (10–30 mW) and fast heat dissipation in the surrounding water medium led to a small increment of the dispersion temperature. Consequently, the localized temperature in hybrid microgels was much higher than that in the dispersion under irradiation. We then visualized the morphology of hybrid microgels after three cycles of laser irradiation. Figure S7, Supporting Information shows that hybrid microgels could retain the core–shell structure with multiple Au nanoparticles trapped on the shell after several shrinking and swelling cycles, which demonstrates the excellent stability and re-usability of this kind of plasmonic hybrid microgel.

As illustrated in Figure 4a,b, the photothermal response of a single droplet was then studied by altering the power and waist of the laser beam. When a single droplet was irradiated by the laser with a relatively small beam waist (6 μm) and low power (8 mW), the hybrid microgels gradually desorbed from the droplet surface (Figure 4e and Movie S1, Supporting Information). Under laser irradiation, Au nanoparticles on the microgel surface were anticipated to absorb light by localized plasmon surface resonance, converting light energy into thermal energy with an associated temperature increase surrounding the microgel (Figure 4a). Accordingly, hybrid microgels underwent a significant volume shrinkage with their surfaces transformed from hydrophilic to hydrophobic at high temperatures (Figure 4c,d). In addition, the increasing thermal energy may overcome the energy needed for microgels to desorb from the oil-water interface, consequently leading to spontaneous microgel desorption and destabilization of the Pickering emulsion. When the droplet was irradiated with increasing laser power (20 mW) and beam waist (30 μm), instantaneous demulsification occurred (Figure 4f and Movie S2, Supporting Information). This phenomenon can be accounted for by the detachment of a significant amount of microgels from a large interfacial area at the same time (Figure 4b). The high thermal energy should also induce a rapid decrease of the interfacial tension between oil and water and generate a strong turbulent flow surrounding the droplet, further facilitating demulsification.

After breaking the Pickering emulsion droplet, a strong photothermal response was also observed even on the broken interfacial film consisting of hybrid microgels, where the hybrid microgel film underwent fast shape deformation under laser irradiation (Figure S8 and Movie S3, Supporting Information). The light-triggered reversible shrinking and swelling of the microgel film were consistent with the above-mentioned result (Figure 2b), further confirming the light-to-thermal transition on

Au@PNIPAM-*co*-ALA microgel surfaces. In contrast, O/W Pickering emulsion droplets stabilized by S-Au@PNIPAM-*co*-ALA microgels did not exhibit an apparent response when irradiated by the focused laser. Only a tiny displacement of small droplets occurred near the laser focus (Movie S4, Supporting Information). We speculate that a single Au nanoparticle inside the microgel matrix was unable to generate sufficient heat to induce microgel collapse and reverse the hydrophilicity.^[49] A theoretical model was established to illustrate the plasmonic photothermal response of a single Au nanoparticle, as seen in Figure S9, Supporting Information. In the simulation, light energy could be rapidly converted to thermal energy around a single Au nanoparticle. However, the generated heat was confined to a few nanometers around the Au nanoparticle due to heat dissipation to the surroundings, consistent with the inapparent photothermal response of S-Au@PNIPAM-*co*-ALA microgel-laden droplets. In contrast, the photothermal response of Au@PNIPAM-*co*-ALA microgels was estimated to be much more pronounced due to the coupling of the plasmonic effect and resultant collective heating.^[50] Since no photothermal response was observed when droplets laden with bare PNIPAM-*co*-ALA microgels were irradiated (Movie S5, Supporting Information), these results suggest that the presence of multiple Au nanoparticles on microgel surfaces is crucial for the light-triggered manipulation of droplets.

To further verify that the wettability of hybrid microgels was indeed altered by the environmental temperature, the contact angle of a water drop on a substrate coated with hybrid microgels in oil was measured at two temperatures. As shown in Figure 4g,h, hybrid microgels exhibited increased hydrophobicity at 50 $^{\circ}\text{C}$ due to the strengthened intermolecular hydrophobic interaction and weakened hydrogen bonding interaction. As a result, it is hard for oil-swollen microgels to intake water molecules at a temperature above the LCST, leading to a relatively constant water contact angle during measurement. On the contrary, at 25 $^{\circ}\text{C}$ which is below the LCST, hybrid microgels are intrinsically hydrophilic. Even though they were immersed and swollen in the oil phase initially, water molecules can gradually permeate into the microgel matrix to compromise the interaction between microgel and oil molecules due to the stronger hydrogen bonding interaction. Consequently, spreading and wetting occurred when the water drop attached to the microgel surface, thus leading to the rapid shape change and significant reduction of water contact angle during measurement. These simulation results and contact angle data further demonstrate that the phenomena observed above regarding hybrid microgel desorption and droplet demulsification were triggered by localized heating.

2.6. Light-Induced Programmable Merging of Droplets

The effect of localized heating on paired emulsion droplets stabilized by Au@PNIPAM-*co*-ALA microgels was subsequently investigated by using a focused 532 nm laser with a 6 μm beam waist and 8 mW power. As shown in Figure 5b and Movie S6, Supporting Information, adjacent droplets instantaneously merged into a larger one upon irradiation by the laser for 0.4 ms. The associated mechanism is illustrated in Figure 5a. Specifically, when the contact interface of paired droplets was irradiated by an intense focused laser, the localized heating raised the temperature

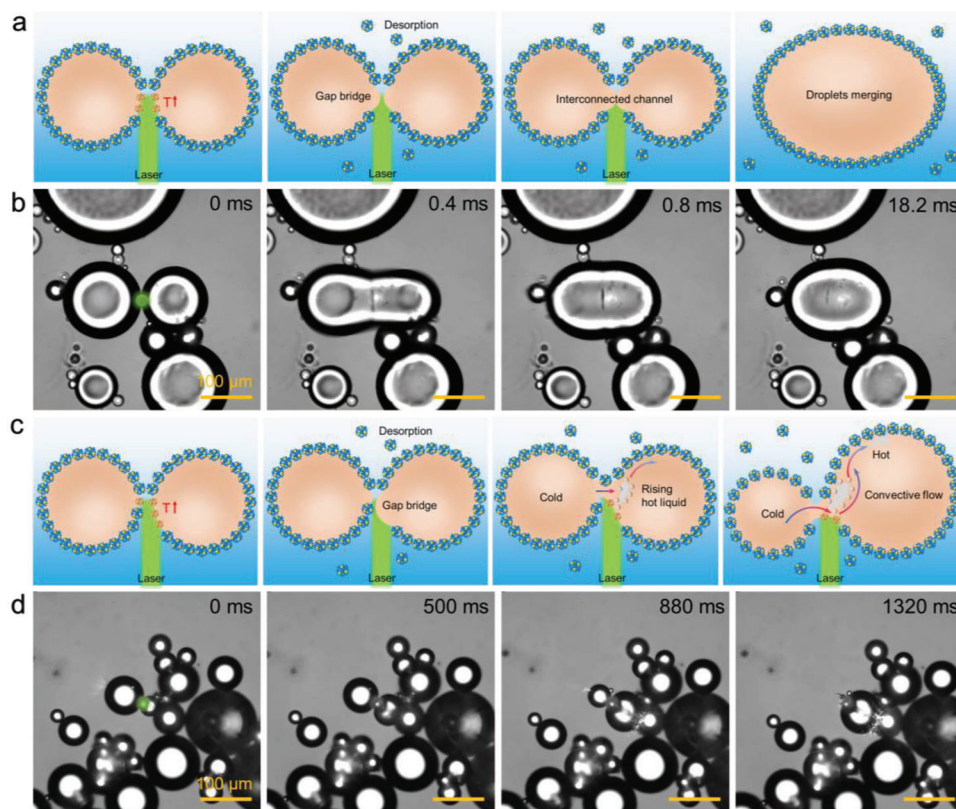


Figure 5. Proposed mechanism for a) droplet merging and c) unidirectional material transfer between adjacent microgel-stabilized oil droplets in water. The process of b) droplet merging and d) material transfer by altering the position of the localized laser on the droplet surface. A focused 532 nm laser with 6 μm beam waist and 8 mW power was used for the irradiation.

to above the LCST and led to the desorption of microgels from the contact interface. Consequently, droplets became sufficiently bridged to initiate the merging process.

With a slight deviation of the laser spot to one droplet, a unidirectional content (the oil phase) transfer is observed as shown in Figure 5d and Movie S7, Supporting Information. The content of the less irradiated droplet (left) gradually transferred into the other one (right), causing apparent volume changes in the two droplets. The content transfer process was observed within the laser exposure of more than 1 sec, which was much longer than the direct droplet merging (Figure 5b). For laser deviation-induced content transfer, the bridging of the two droplets was insignificant as only a small fraction of microgels detached from the interface of the less irradiated droplets, retaining the structural stability of the droplet (Figure 5c). During the irradiation, cavitation of small vapor bubbles was also observed inside the oil droplet, suggesting that the oil phase was superheated and the temperature at the localized spot reached the boiling point of toluene.^[51] The unique content transfer behavior is anticipated from the Marangoni flow around the vapor bubble and thermal convection flow inside the droplet, whereby the content moved from the colder droplet to the hotter one. This unidirectional transfer process lasted until the less irradiated droplet became exhausted. These results indicate that the photo-responsive behavior of paired droplets stabilized by Au@PNIPAM-co-ALA microgels can be controlled by altering the position of the focused laser.

However, a more systematic investigation is required to achieve precise control.

2.7. Chemical Communication between Adjacent Pickering Emulsion Droplets

Subsequently, we investigated whether chemical communication between droplets may be possible by light-induced droplet merging. Before laser irradiation, two types of oil droplets containing dye molecules of Nile red or perylene were prepared, showing red and blue color in fluorescence images, respectively. The Au@PNIPAM-co-ALA microgels were pre-stained by fluorescein isothiocyanate shown in green fluorescence. It was observed that neither merging nor content exchange occurred when two droplets were in contact (Figure 6a). Upon localized heating by laser irradiation, however, two adjacent droplets containing different dye molecules immediately merged and the encapsulated dye molecules were mixed, showing a violet color (Figure 6b). Additionally, the microgels were rearranged on the surface of the merged droplet to maintain droplet stability. By contrast, droplets not exposed to laser irradiation retained structural integrity without content exchange. Corresponding to the observed phenomenon, the fluorescence profiles indicate that the fluorescence intensity and distribution of contacted adjacent droplets changed significantly after irradiation, whereas no apparent

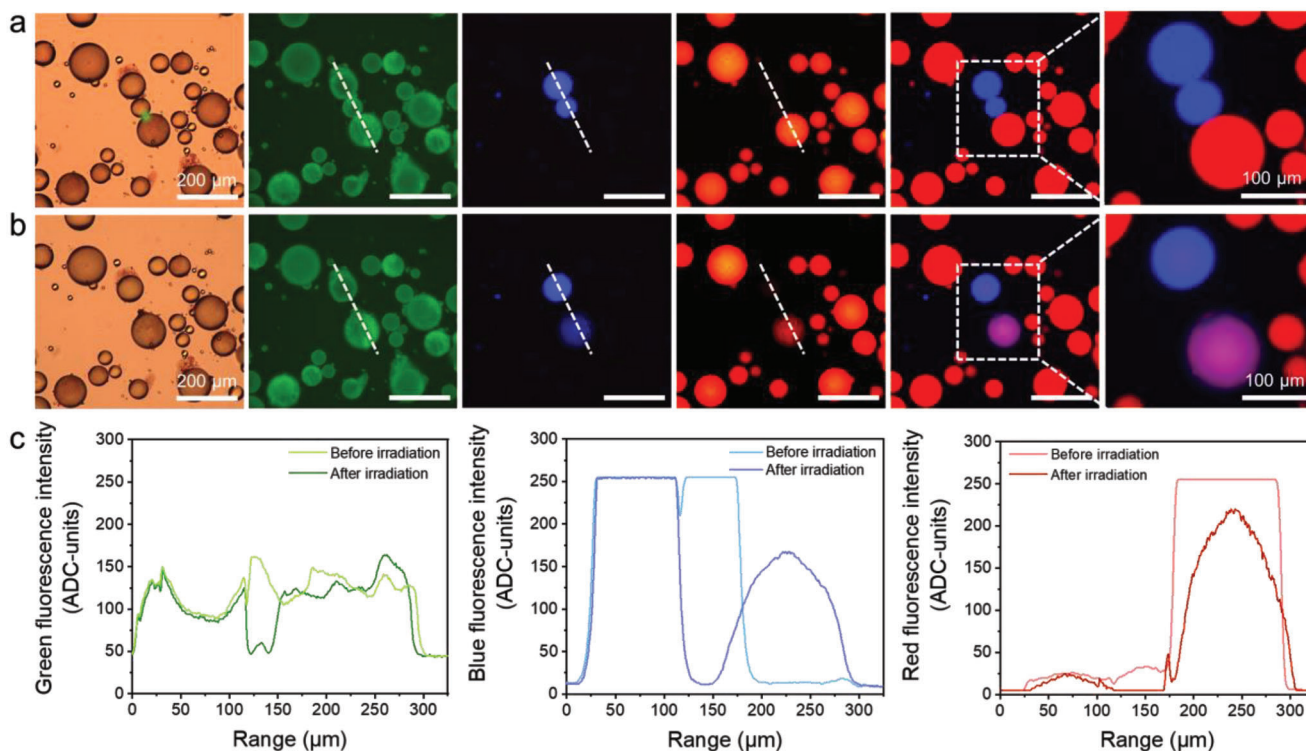


Figure 6. Chemical communication between adjacent O/W Pickering emulsion droplets containing either perylene or Nile red dye molecules stabilized by Au@PNIPAM-co-ALA microgels. Fluorescence images for adjacent droplets a) before and b) after laser irradiation. c) Corresponding fluorescence intensity profiles of three adjacent droplets along the dashed lines before and after laser irradiation.

differences in fluorescence were observed in droplets without irradiation within the measuring range (Figure 6c). These results demonstrate that the light-driven merging between droplets stabilized by Au@PNIPAM-co-ALA microgels may trigger chemical communication between two microreactors for potential control of chemical reactions at high temporal resolution.

2.8. Design of Artificial Microswimmer Templated from Air-Containing O/W Pickering Emulsion Droplets

In addition to light-induced demulsification and chemical communication between droplets, air bubble generation was observed inside the droplets under focused laser irradiation for extended periods. As shown in Figure 7a,b, the localized heat accumulated around the interior interface induced the cavitation of small vapor bubbles. After the collapse of microbubbles, a new bubble formed and started to grow due to the vaporization of the superheated surrounding oil phase (Movie S8, Supporting Information). Two possible reasons why the explosive bubble appeared inside the oil phase instead of the water phase are: First, at room temperature (25 °C) and standard pressure (0.101 MPa), the thermal conductivity and specific heat capacity of toluene are 0.13 W/(m K) and 1.70 kJ/(kg K), while water features a much higher thermal conductivity (0.60 W/(m K)) and specific heat capacity (4.18 kJ/(kg K)). Due to the poor heat diffusion of the oil phase, heat more easily accumulates in toluene than in water, resulting in a more significant temperature increase in the oil

phase. Second, the oil phase is highly gas-rich compared with the water phase. The aggregation of gas molecules can serve as a nucleus for bubble generation, thereby reducing the nucleation temperature. Hence, even though the boiling point of toluene (110.6 °C) is slightly higher than that of water (100 °C) at 0.101 MPa, explosive bubbles may be generated more readily in toluene.

As the bubble was generated only inside the oil droplet, an air-in-oil-in-water (A/O/W) emulsion droplet was obtained under laser irradiation (Figure 7b). Importantly, we found that the movement of the A/O/W droplet could be precisely manipulated by laser irradiation. In other words, the trajectory of the A/O/W droplet was directed by the laser, which can achieve communication between isolated droplets and demonstrate the potential of designing the A/O/W droplet as an artificial microswimmer mimicking the behavior of an aquatic creature in a fluid environment. Figure 7c and Movie S9, Supporting Information show the detailed manipulation process. When the laser was moved at a constant velocity, the A/O/W droplet may track it up to an escape velocity, leading to the capture of a target droplet by touching and merging. The growing microswimmer may be continuously moved by the laser. When the laser stopped moving, the droplet motion also stopped and re-centered around the laser focus. It should be noted that the bubble inside the droplet gradually vanished after turning off the laser due to the dissipation of accumulated heat.

The observed phenomenon may be further elucidated by the collective heating effect of the laser beam, inducing upward hot

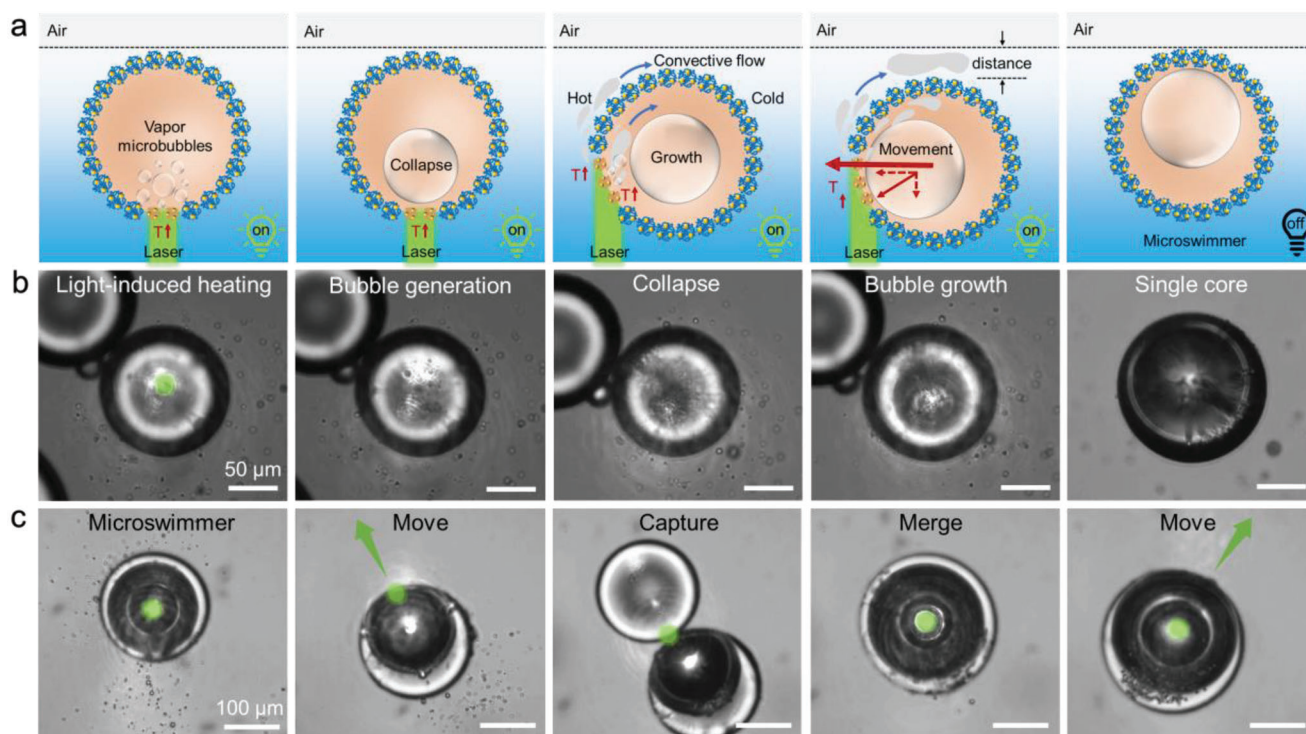


Figure 7. a) Proposed mechanism and b) corresponding optical microscopy images of bubble generation, collapse and growth processes inside a O/W Pickering emulsion droplet when irradiated by the laser for a prolonged period. c) Spatiotemporal manipulation of an artificial microswimmer: A/O/W droplet. A focused 532 nm laser with a 6 μm beam waist and 8 mW power was used for irradiation.

liquid and convective flows dragging the droplet surface along (Figure 7a). Although the laser was focused on the lower part of the droplet, the generated convective flow was developed and resembled on top of the heated area of the droplet, giving rise to a horizontal driving force.^[40,52] As a result, both the inner air bubble and the oil droplet are attracted to the center of the laser spot. In addition, we speculate that the upward convective flow may increase the distance between the air-water interface and the droplet, thereby reducing the interfacial resistant force. Hence, the attraction force collectively generated by the convective flow and the reduced resistance enabled the light-driven spatiotemporal movement of a droplet.

3. Conclusion

In this work, we present a novel strategy for light-driven Pickering emulsion droplet manipulation enabled by plasmonic hybrid Au@PNIPAM-co-ALA microgels, which are co-assembled by oppositely charged PNIPAM-co-ALA microgels and Au nanoparticles via electrostatic heterocoagulation. Taking advantage of the plasmonic photothermal response of Au nanoparticles and the thermal sensitivity of PNIPAM-based microgels, the “cascade effect” of laser irradiation induces the hybrid microgels to transform from hydrophilic to hydrophobic, allowing precise manipulation of the droplet behaviors, including microgel desorption, demulsification, droplet merging and inner bubble generation by simply altering the beam waist and power of the applied laser. Moreover, the movement of an A/O/W emulsion droplet may be spatiotemporally manipulated by light, showing the potential

as an artificial microswimmer. Besides, chemical communication between isolated droplets triggered by laser irradiation has also been demonstrated. We envisage that the presented system may open new possibilities for studies and applications requiring on-demand substance transport, programmed release and controlled catalytic reactions.

Supporting Information

Supporting Information is available from the Wiley Online Library or from the author.

Acknowledgements

The authors gratefully acknowledge the financial support provided by the Research Grants Council of Hong Kong Special Administration Region, HKSAR (Project Nos. CUHK14304619, CUHK14204820, 2130642), the Hong Kong Innovation and Technology Fund (Grant No. ITS/217/21) as well as the VC Discretionary Fund provided by The Chinese University of Hong Kong (Project No. 8601014). [Correction added after publication 22 November 2023: Reference list was corrected.]

Conflict of Interest

The authors declare no conflict of interest.

Author Contributions

X.G. and G.Y.C. contributed equally to this work. X.G.: conceptualization, methodology, investigation, formal analysis, and writing – original draft.

G.Y.C.: investigation, formal analysis, simulation, review and editing. Y-P.H. and B.P.B.: review and editing, and supervision. T.N.: conceptualization, writing – review and editing, project administration, and supervision

Data Availability Statement

The data that support the findings of this study are available from the corresponding author upon reasonable request.

Keywords

light-driven droplet manipulation, photothermal effect, Pickering emulsion, plasmonic hybrid microgels

Received: May 20, 2023
Revised: July 13, 2023
Published online: July 25, 2023

- [1] S. U. Pickering, *J. Chem. Soc.* **1907**, 91, 2001.
[2] H. Jiang, Y. Sheng, T. Ngai, *Curr. Opin. Colloid Interface Sci.* **2020**, 49, 1.
[3] I. Navarro Arrebola, L. Billon, G. Aguirre, *Adv. Colloid Interface Sci.* **2021**, 287, 102333.
[4] M. Rey, M. A. Fernandez-Rodriguez, M. Karg, L. Isa, N. Vogel, *Acc. Chem. Res.* **2020**, 53, 414.
[5] Z. Li, T. Ming, J. Wang, T. Ngai, *Angew. Chem., Int. Ed.* **2009**, 48, 8490.
[6] S. Stock, R. von Klitzing, *Curr. Opin. Colloid Interface Sci.* **2022**, 58, 101561.
[7] M. A. Fernandez-Rodriguez, A. Martin-Molina, J. Maldonado-Valderrama, *Adv. Colloid Interface Sci.* **2020**, 288, 102350.
[8] S. A. Deshmukh, S. K. Sankaranarayanan, K. Suthar, D. C. Mancini, *J. Phys. Chem. B* **2012**, 116, 2651.
[9] L. J. Abbott, A. K. Tucker, M. J. Stevens, *J. Phys. Chem. B* **2015**, 119, 3837.
[10] Y. Ma, S. Ma, Y. Wu, X. Pei, S. N. Gorb, Z. Wang, W. Liu, F. Zhou, *Adv. Mater.* **2018**, 30, 1801595.
[11] S. Wiese, A. C. Spiess, W. Richtering, *Angew. Chem., Int. Ed.* **2013**, 52, 576.
[12] F. A. Plamper, W. Richtering, *Acc. Chem. Res.* **2017**, 50, 131.
[13] F. Li, C. Wang, W. Guo, *Adv. Funct. Mater.* **2018**, 28, 1705876.
[14] R. A. Meurer, S. Kemper, S. Knopp, T. Eichert, F. Jakob, H. E. Goldbach, U. Schwaneberg, A. Pich, *Angew. Chem., Int. Ed.* **2017**, 56, 7380.
[15] A. Seyfoori, S. A. Seyyed Ebrahimi, E. Samiei, M. Akbari, *ACS Appl. Mater. Interfaces* **2019**, 11, 24945.
[16] Y. Wang, L. Zhu, H. Zhang, H. Huang, L. Jiang, *Carbohydr. Polym.* **2020**, 241, 116373.
[17] S. Hackelbusch, T. Rossow, D. Steinhilber, D. A. Weitz, S. Seiffert, *Adv. Healthcare Mater.* **2015**, 4, 1841.
[18] M. Karg, T. Hellweg, *Curr. Opin. Colloid Interface Sci.* **2009**, 14, 438.
[19] D. Suzuki, C. Kobayashi, *Langmuir* **2014**, 30, 7085.
[20] M. Tagliacucchi, F. Zou, E. A. Weiss, *J. Phys. Chem. Lett.* **2014**, 5, 2775.
[21] X. Guan, J. Wei, Y. Xia, T. Ngai, *ACS Macro Lett.* **2022**, 11, 1014.
[22] H. Jiang, S. Zhang, G. Sun, Y. Li, X. Guan, C. Yang, T. Ngai, *Chem. Sci.* **2021**, 13, 39.
[23] J. Pérez-Juste, I. Pastoriza-Santos, L. M. Liz-Marzán, *J. Mater. Chem. A* **2013**, 1, 20.
[24] K. Wiemer, K. Dormbach, I. Slabu, G. Agrawal, F. Schrader, T. Caumanns, S. D. M. Bourone, J. Mayer, J. Steitz, U. Simon, A. Pich, *J. Mater. Chem. B* **2017**, 5, 1284.
[25] W. Wu, J. Liu, P. Gong, Z. Li, C. Ke, Y. Qian, H. Luo, L. Xiao, F. Zhou, W. Liu, *Small* **2022**, 18, 2202510.
[26] R. Contreras-Cáceres, A. Sánchez-Iglesias, M. Karg, I. Pastoriza-Santos, J. Pérez-Juste, J. Pacifico, T. Hellweg, A. Fernández-Barbero, L. M. Liz-Marzán, *Adv. Mater.* **2008**, 20, 1666.
[27] B. Brugger, W. Richtering, *Adv. Mater.* **2007**, 19, 2973.
[28] S. Backes, M. U. Witt, E. Roeben, L. Kuhrt, S. Aleed, A. M. Schmidt, R. von Klitzing, *J. Phys. Chem. B* **2015**, 119, 12129.
[29] L. Tzounis, M. Dona, J. M. Lopez-Romero, A. Fery, R. Contreras-Caceres, *ACS Appl. Mater. Interfaces* **2019**, 11, 29360.
[30] D. Boyaciyan, R. von Klitzing, *Curr. Opin. Colloid Interface Sci.* **2019**, 44, 193.
[31] M. Lehmann, W. Tabaka, T. Moller, A. Oppermann, D. Woll, D. Volodkin, S. Wellert, R. V. Klitzing, *Langmuir* **2018**, 34, 3597.
[32] M. Wei, M. J. Serpe, *Part. Part. Syst. Charact.* **2019**, 36, 1800326.
[33] H. Wu, X. Du, X. Meng, D. Qiu, Y. Qiao, *Nat. Commun.* **2021**, 12, 6113.
[34] M. Zhang, R. Ettlai, L. Dong, X. Li, T. Li, X. Zhang, B. P. Binks, H. Yang, *Nat. Commun.* **2022**, 13, 475.
[35] D. Dedovets, Q. Li, L. Leclercq, V. Nardello-Rataj, J. Leng, S. Zhao, M. Pera-Titus, *Angew. Chem., Int. Ed.* **2022**, 61, e202107537.
[36] X. Guan, Z. Wan, T. Ngai, *Aggregate* **2022**, 4, e300.
[37] C. Y. Xie, S. X. Meng, L. H. Xue, R. X. Bai, X. Yang, Y. Wang, Z. P. Qiu, B. P. Binks, T. Guo, T. Meng, *Langmuir* **2017**, 33, 14139.
[38] L. Hou, Y. Ren, Y. Jia, X. Deng, W. Liu, X. Feng, H. Jiang, *ACS Appl. Mater. Interfaces* **2017**, 9, 12282.
[39] S.-Y. Park, P.-Y. Chiou, *Adv. Optoelectron.* **2011**, 2011, 909174.
[40] Z. Yang, J. Wei, Y. I. Sobolev, B. A. Grzybowski, *Nature* **2018**, 553, 313.
[41] G. Cheng, K. T. Lin, Y. Ye, H. Jiang, T. Ngai, Y. P. Ho, *ACS Appl. Mater. Interfaces* **2021**, 13, 21914.
[42] D. G. Grier, *Nature* **2003**, 424, 810.
[43] C. N. Baroud, J. P. Delville, F. Gallaire, R. Wunenburger, *Phys. Rev. E: Stat. Nonlinear Soft Matter Phys.* **2007**, 75, 046302.
[44] C. N. Baroud, M. R. de Saint Vincent, J. P. Delville, *Lab Chip* **2007**, 7, 1029.
[45] X. Chen, T. Wu, D. Huang, J. Zhou, F. Zhou, M. Tu, Y. Zhang, B. Li, Y. Li, L. Jiang, *Adv. Mater.* **2022**, 34, 2205563.
[46] F. Wang, M. Liu, C. Liu, C. Huang, L. Zhang, A. Cui, Z. Hu, X. Du, *Nat. Sci. Rev.* **2023**, 10, nwac164.
[47] G. Agrawal, M. P. Schürings, P. van Rijn, A. Pich, *J. Mater. Chem. A* **2013**, 1, 13244.
[48] H. Hwang, P. Papadopoulos, S. Fujii, S. Wooh, *Adv. Funct. Mater.* **2022**, 32, 2111311.
[49] M. Barella, I. L. Violi, J. Gargiulo, L. P. Martinez, F. Goschin, V. Guglielmotti, D. Pallarola, S. Schlucker, M. Pilo-Pais, G. P. Acuna, S. A. Maier, E. Cortes, F. D. Stefani, *ACS Nano* **2021**, 15, 2458.
[50] G. Baffou, P. Berto, E. Bermúdez Ureña, R. Quidant, S. Monneret, J. Polleux, H. Rigneault, *ACS Nano* **2013**, 7, 6478.
[51] M. E. Zaytsev, G. Lajoinie, Y. Wang, D. Lohse, H. J. W. Zandvliet, X. Zhang, *J. Phys. Chem. C* **2018**, 122, 28375.
[52] N. D. Dinh, R. Luo, M. T. A. Christine, W. N. Lin, W. C. Shih, J. C. Goh, C. H. Chen, *Small* **2017**, 13, 1700684.